LA-UR- 97-503

CONF-970597--1

Los Alamos National Laboratory is operated by the University of California for the United States Department of Energy under contract W-7405-ENG-36.

TITLE: EXPLORING THE CONFORMATIONAL ENERGY LANDSCAPE OF PROTEINS

AUTHOR(S): G. Ulrich Nienhaus, University of Illinois at Urbana and Universitat Ulm
Joachim D. Muller, University of Illinois at Urbana
Ben H. McMahon, University of Illinois at Urbana
Hans Frauenfelder, CNLS/T-Division

SUBMITTED TO CNLS proceedings "Landscape Paradigms" May 13-17. 1996
Los Alamos National Laboratory, Los Alamos, NM 87545

Los Alamos

Los Alamos National Laboratory
Los Alamos, New Mexico 87545

FORM NO. 836 R4
ST. NO. 2629 5/81

DISCLAIMER

Exploring the conformational energy landscape of proteins

G. Ulrich Nienhaus [a,b,1], Joachim D. Müller [a], Ben H. McMahon [a], and Hans Frauenfelder [c]

[a] *Department of Physics, University of Illinois at Urbana-Champaign, 1110 West Green Street, Urbana, IL 61801, USA,*

[b] *Department of Biophysics, Universität Ulm, D-89069 Ulm, Germany,*

[c] *Center for Nonlinear Studies, Los Alamos National Laboratories, Los Alamos, NM 87545, USA.*

Proteins possess a complex energy landscape with a large number of local minima called conformational substates that are arranged in a hierarchical fashion. Here we discuss experiments aimed at the elucidation of the energy landscape in carbonmonoxy myoglobin (MbCO). In the highest tier of the hierarchy, a few taxonomic substates exist. Because of their small number, these substates are accessible to detailed structural investigations. Spectroscopic experiments are discussed that elucidate the role of protonations of amino acid side chains in creating the substates. The lower tiers of the hierarchy contain a large number of statistical substates. Substate interconversions are observed in the entire temperature range from below 1 K up to the denaturation temperature, indicating a wide spectrum of energy barriers that separate the substates.

Key words: Protein Dynamics, Conformational Substates, Energy Landscape, Myoglobin, Infrared Spectroscopy

[1] Address correspondence to: Dr. Gerd Ulrich Nienhaus, Dept. of Biophysics, Universität Ulm, D-89069 Ulm, Germany. Tel.: +49-731-502-3050, Fax: +49-731-502-3059, Email: uli@uiuc.edu.

1 Introduction

The 16^{th} Annual CNLS Conference brought together scientists interested in a wide and diverse spectrum of fields, including glasses, spin glasses, biopolymers, neural networks, and evolution. In all these areas, the systems under study can be characterized by an enormously complex state space, and the overarching paradigm of the conference, the rugged energy landscape, allows one to organize and classify the large number of states. While there is impressive activity in theory and computational efforts in this field, detailed experimental investigations aimed at the elucidation of complex energy landscapes are still rare.

Proteins are especially useful systems for experimental studies of complexity for several reasons: They are accessible to structure analysis with x-rays, neutrons, and NMR, whereas for glasses and synthetic polymers, data in the intermediate distance range (8-50 Å) are difficult to obtain. Proteins are still small enough that local properties can be studied, and powerful tools of genetic engineering can be employed to selectively modify individual groups of atoms. Moreover, the functional properties are sensitive probes of the structure and dynamics of proteins.

In this paper, we give an overview of the hierarchical energy landscape in carbonmonoxy myoglobin (MbCO). While MbCO can exist in a huge number of different *conformational substates*, it exhibits a few easily distinguishable conformations in the highest tier (CS0) of the hierarchy, the so-called taxonomic substates. We discuss structural, dynamic, and functional aspects associated with the taxonomic substates. We present new infrared-spectroscopic data that show the importance of protonations in the furcation of the energy landscape. In addition, we also discuss the experimental evidence for the large number of *statistical substates* in the lower tiers of the hierarchy.

2 Protein structure

Proteins are linear, unbranched polymers of amino acids linked by (covalent) peptide bonds [1]. The sequence of amino acids is called the primary structure. The amino acid chain folds into secondary structure elements, the most important of which are the α-helices and β-pleated sheets. The helices and sheets are packed against each other in the compact, three-dimensional structure (tertiary structure) that is held together by noncovalent forces (except for the occasionally occurring disulfide bridges), van der Waals forces, hydrogen bonds, salt bridges, and hydrophobic interactions [2].

The biologically active, native structure exhibits considerable structural variability

that endows the protein with the capability to perform its functional tasks. The dense packing in the interior of a protein molecule, which is comparable to that of typical crystals of organic molecules, results in competition of groups of atoms for the same space. Consequently, frustrated interactions occur, analogous to the phenomena found in spin glasses [3,4]. A helix may be blocked from sliding or bending by other helices or residues. Groups of atoms in a protein molecule are locked in, or sterically hindered, by neighboring groups of atoms and cannot move unless the neighbors move first. Steric hindrance thus plays an essential role, and rearrangement of the structure is a highly cooperative process. Proteins are examples of systems with constrained dynamics [5]. The aperiodic structure and the presence of frustration results in the rugged energy landscape of the protein molecule, and the hierarchy of structural constraints results in a hierarchically-arranged energy landscape [6–11].

3 Hierarchical energy landscape of proteins

Different proteins possess different conformational energy landscapes. However, since all proteins are built according to the same construction principle, their energy landscapes may show universal concepts and features. Consequently, we use myoglobin (Mb) as a prototype for exploring the conformational energy landscape of proteins.

Mb, the oxygen storage protein in muscle, consists of 153 amino acids. It has a molecular weight of 17.8 kDa and the approximate dimensions $2.5 \times 3.5 \times 4.5$ nm^3 (Fig. 1). The folded polypeptide chain surrounds a heme group with a central iron atom, which reversibly binds small ligands such as O_2 and CO. The structure of Mb includes an interior volume, the heme pocket, that contains the ligand binding site. Some of the most compelling evidence for the complex structure and dynamics of proteins comes from monitoring the rebinding of ligands to myoglobin (and other heme proteins) after photodissociation. In particular, carbonmonoxy myoglobin (MbCO) has been studied in great detail. In the simplest picture, the ligand binding reaction is described by a three-well model, so that upon ligand binding, the system has to overcome two successive barriers; the first one is connected with ligand entry to or exit from the heme pocket, and the second one is associated with bond formation. During the reaction, equilibrium fluctuations and nonequilibrium relaxations affect the binding kinetics in characteristic ways. Consequently, protein motions can be investigated through the ligand binding reaction. Mb is simple enough that its substates and motions can be studied in detail yet complex enough that the concepts found may be valid for most or even all proteins.

The arrangement of conformational substates in carbonmonoxy myoglobin (MbCO) is

visualized schematically in Fig. 1 [6,7,9], where the conformational potential energy E_c of the protein is plotted as a function of a (conceptual) conformational coordinate. Of course, the energy landscape is actually a hypersurface in the high-dimensional space of the coordinates of all atoms in the protein as well as in the hydration shell. It has structure on several energy and length scales and exhibits a hierarchical arrangement of conformational substates: the CSi denotes the substates in the i-th tier in the hierarchy. The top row shows MbCO as a conformational state with a unique structure corresponding to a single energy minimum. The hierarchy of MbCO furcates into several tiers. Tiers 0 and 1 are well established by a variety of experiments that will be discussed below. The existence of lower tiers is also implied by experiments, but the classification appears much more problematic.

3.1 Taxonomic substates

The infrared (IR) spectrum of sperm whale MbCO shows a few discrete stretch bands of the bound CO ligand, which are denoted A_0, A_1, A_3, with peak wavenumbers $\nu(A_0) \approx 1966$ cm^{-1}, $\nu(A_1) \approx 1945$ cm^{-1}, $\nu(A_3) \approx 1933$ cm^{-1}. The different IR bands arise from the presence of different structural environments of the bound CO ligand. Since the number of these substates is small, they can be individually characterized, and we refer to them as *taxonomic substates* [9]. They are assigned to tier 0 of the substate hierarchy (CS0). The relative populations and individual properties of the CS0 substates are affected differently by external agents including temperature [7,12,13], pressure [14], pH [13,15], and solvent environment [16]. Moreover, the CO binding kinetics at low temperatures are different if monitored in the three A bands (Fig. 2a) [7,17].

3.1.1 Structure

The presence of a few distinct taxonomic substates raises questions concerning the structural determinants that lead to the furcation of the energy landscape into separate basins. Substantial insights have been obtained by investigating the response of the protein to variation of the proton concentration in the environment. The uptake or release of a proton is a significant perturbation that can affect the CO stretch vibration in heme proteins through different mechanisms: by alteration of the arrangement of amino acids near the CO, electrostatic interactions between the CO and the protonated residue, hydrogen bonding, or polarization of the extended π-electron system of the heme group. Fig. 3 shows that the A substate spectrum changes in a characteristic way with pH. At high pH, A_1 and A_3 predominate. With decreasing pH,

the population of A_0 grows at the expense of the other two A states. A second effect is an up-shift of the individual peak wavenumbers by 2 – 3 cm with decreasing pH. Protonation of amino acid residues are responsible for these pH-dependent changes of the IR spectra.

Protonation changes of amino acid side chains are often key steps in the functional action of enzymes. Among the amino acids, histidine plays a special role because its imidazole side chain titrates near neutral pH. In myoglobin, there are three histidines near the active site, His64, His93, and His97, as sketched in Fig. 4. His93, the proximal histidine, provides the covalent link of the heme group to the polypeptide chain and is known to be unprotonated in the pH range considered here [18,19]. His64 is called the distal histidine. At neutral pH, its imidazole side chain is close to the CO ligand in the heme pocket, and recent studies of site-specific mutants of MbCO have shown that most of the dispersion of the stretch frequencies in the A states is due to interactions of the bound CO with the imidazole side chain [20,21]. The third histidine, His97, is located on the proximal side of the heme disk. With two single-site mutants, His64Val and His97Phe, which each have one of the histidines replaced by non-protonating residues, valine and phenyl alanine, respectively, we were able to prove that the observed pH dependence of the spectra is explained by titrations of His64 and His97 [22] (and manuscript in preparation). In these two mutants, the protonations can be studied separately, whereas in native MbCO, they appear concomitantly, with His64 and His97 having pK values of 4.4 and 6.0, respectively.

We introduce four different conformational substates to represent the two protonation states of the two residues, as sketched in Fig. 5. At low pH, S_{11}, with both histidines protonated, predominates, whereas at high pH, the entire population exists in S_{00}, where both histidines are unprotonated. In the intermediate range, the mixed states, S_{01} and S_{10} are present, but S_{01}, with protonated His97, is much more abundant. Taking the amplitudes of the four species in Fig. 4, we can indeed model the pH dependence of the IR spectra in Fig. 3 a as linear superpositions of the basis spectra of the individual protonation states that are plotted in Fig. 3 b. This simple model is sufficient to describe the data; introducing additional states, as suggested in earlier studies [23], proved unnecessary in the analysis. Note that there are only three basis spectra because the two mixed species S_{01} and S_{10} occur in a fixed ratio at all pH values so that they cannot be obtained independently from pH variation. However, since S_{10} contributes only 3 % to the mixed species, the intermediate spectrum is essentially that of S_{01}.

We emphasize some differences of this approach to earlier work on the A substates [7]. Previously, the taxonomic substates were characterized according to the positions

of the three main CO stretch bands, A_0, A_1, and A_3. In the present analysis, we use the pH dependence of the IR spectra to separate four substates, defined through the protonation states of two histidine residues, 64 and 97. The entire IR spectrum is affected by the protonation, so the different species are not characterized by individual IR bands. Fig. 3 b shows that the dominant absorption of the doubly protonated species occurs at 1966 cm^{-1} and so A_0 is a good though not perfect marker for this species. Indeed, if the imidazole side chain of His64 is protonated, the CO absorbs in the A_0 band; if His64 is deprotonated, the CO absorbs either in A_1 or A_3. However, there are also contributions of the S_{11} species at lower wavenumbers, even at the A_1 position. The influence of His97 on the IR spectra is different in nature: If His97 is protonated, the CO absorbs at $2-3$ cm^{-1} higher than if it is in the unprotonated form. The dependence may also explain the observed shifts of the A bands with pressure and temperature [7,14], which can now at least in part be attributed to variations in the protonation state of His97.

Obviously, protonation reactions can create taxonomic substates. However, they are not the only mechanisms, as is evident from the behavior of A_1 and A_3. The population ratio of these two substates is independent of pH, and thus they occur as one species in our four-state scheme. The separation of these two states must have a different reason, for example a double-minimum potential created by adjacent residues.

Recent x-ray diffraction experiments of MbCO have given direct evidence for the structural alterations that accompany the protonation of His64. Earlier IR experiments showed that mutants where His64 was replaced by amino acids with short, apolar side chains absorb near 1966 cm^{-1} similar to A_0 [20,21]. Therefore, it was expected that, upon protonation, the His64 side chain changes its conformation and turns towards the solvent, leaving behind an apolar heme pocket. Indeed, the x-ray structure of MbCO at pH 4, where A_0 is dominant, shows that the His64 side chain has swung out of the distal pocket [24,25].

3.1.2 Dynamics

Interconversion between the taxonomic substates can been measured by relaxation spectroscopy, where a perturbation forces the sample rapidly out of equilibrium, and the subsequent relaxation towards equilibrium is followed spectroscopically by monitoring an observable, $M(t,T)$, for example, the area of an A substate band, or the peak absorption, as function of time t and temperature T.

We have employed two different techniques to study A substate interconversions. For characteristic times of 100 s or more, hydrostatic pressure was applied to the samples

to change the relative A state populations because of their different volumes. This was done at temperatures sufficiently high for a quick response. Then the sample was cooled down to temperatures where the response was sufficiently slow so that the relaxation after a sudden release of pressure could be measured by FTIR spectroscopy. The change in the area of the A substate bands was parametrized by a relaxation function $\Phi(t,T)$, defined by

$$\Phi(t,T) = \frac{M(t,T) - M(\infty,T)}{M(0,T) - M(\infty,T)}. \tag{1}$$

$M(0,T)$ is the value of $M(t,T)$ immediately after the perturbation, and $M(\infty,T)$ is the value of the observable when the new equilibrium is reached.

The time dependence of the relaxation function in proteins is often well approximated by a stretched exponential [26]

$$\Phi(t,T) = \exp(-[\kappa(T)t]^{\beta}), \tag{2}$$

where $0 < \beta < 1$. The exponent is frequently found in the range 0.3 - 0.5. For the A state exchange, however, the relaxation functions were close to exponential, so the apparent rate coefficients were determined from fits of exponentials to the relaxation functions.

To measure relaxation on faster time scales, flash photolysis with IR monitoring at the peak wavenumbers of the A substates was used [7,17,27]. Below $\approx$150 K, transitions between the A substates do not occur on any experimental time scale, and nonexponential rebinding of the individual A substates is observed, as shown in Fig. 2 a for $T = 120$ K. The kinetics can be modelled with different activation enthalpy distributions, plotted in Fig. 2 b. The significantly different rebinding kinetics in the three A substates enables one to study transitions between these substates because it creates a nonequilibrium population at times small compared with the exchange rates. At longer times, equilibrium is established.

After the photolysis pulse, rebinding occurs within each substate separately as long as the time has not exceeded the characteristic time for A substate interconversion. Because A_3 has the highest barriers, it will rebind slowest and become underpopulated with respect to equilibrium. As the experimental time scale crosses the characteristic time for interconversion, equilibrium is restored by thermal transitions from A_1 (Exchange with A_0 does not play a role because this process is much slower, see below). For times longer than the transitions, the rebinding kinetics becomes identical in each of the three A substates. The time where the kinetic traces merge can be taken as an

estimate for the interconversion rate.

In the A_0 substate, this kinetic generation of a non-equilibrium situation gives rise to quite a spectacular kinetic behavior, as shown in Fig. 6. At these temperatures, the kinetics of A_0 are very peculiar: After a rebinding phase, the $N(t)$ traces turn up again on an intermediate time scale before they finally decay. The only reasonable way to explain the loss of A_0 population on intermediate time scales involves transitions among the taxonomic substates. In this process, A_1 and A_3 appear as a single kinetic species because they interconvert much faster.

We extract rate distribution from the kinetics data and characterize the A substate transitions with an average rate coefficient, κ, given by the peak position of this distribution [17,28]. Fig. 7 shows the temperature dependence of κ, plotted logarithmically as a function of $(1000/T)^2$. This plot implies that the relation introduced by Ferry et al. [29],

$$\kappa(T) = A_F \exp[-(E_F/RT)^2], \tag{3}$$

and not the usual Arrhenius relation,

$$\kappa(T) = A\frac{T}{T_0}\exp[-(E/RT)], \tag{4}$$

is appropriate for describing the temperature activation of these protein motions. Equation 3 was originally introduced empirically. It is also obtained as a result of the Gaussian random energy model [30–34]. A fit with Eq. 4 yields an activation enthalpy of 90 kJ/mol and a preexponential of $10^{21.6}$ s^{-1} for the $A_0 \leftrightarrow A_1 + A_3$ transition, and 118 kJ/mol and $10^{30.2}$ s^{-1} for $A_1 \leftrightarrow A_3$. The high enthalpies and preexponentials clearly show that these protein interconversions are complex phenomena, and not single barrier crossings of the Arrhenius type. With Eq. 3, E_F = 9.3 kJ/mol and $A_F = 10^{11.8}$ s^{-1} for the $A_0 \leftrightarrow A_1 + A_3$ transition, and E_F = 9.9 kJ/mol and $A_F = 10^{16.4}$ s^{-1} for $A_1 \leftrightarrow A_3$.

The very different time scales of the two interconversion processes in Fig. 7 allow further speculation about the nature of the structural transitions that accompany these motions. In crystals at pH 7, only the A_1 and A_3 substates are populated, and the x-ray structure shows the His64 imidazole side chain buried inside the heme pocket. In the x-ray structure at pH 4, the side chain has turned out of the heme pocket into the solvent [24,25]. Consequently, the $A_0 \leftrightarrow A_1 + A_3$ transition involves cooperative motions of the protein and the surrounding solvent that allow the imidazole side chain to swing out of the heme pocket. Therefore, it is not surprising that this motion is

comparatively slow, and it is also strongly dependent on the solvent viscosity [27]. The interconversion rate coefficient of $A_1 \leftrightarrow A_3$ is more than 3 orders of magnitude faster than the $A_0 \leftrightarrow A_1 + A_3$ exchange; extrapolation of the $A_1 \leftrightarrow A_3$ rate to room temperature yields about 1 ns. The much faster interconversion suggests that less structural reorientation is necessary than in the $A_0 \leftrightarrow A_1 + A_3$ process.

From the kinetics data, the most likely structural model of the A_1 and A_3 substates has the imidazole side chain of His64 in the same configuration, with a proton attached to N_ϵ in both A_1 and A_3. Subtle interactions between His64 and its environment lead to one substate, A_1, with less and one substate, A_3, with more interaction between the proton and the CO. Different amounts of down-shift of the IR lines from the A_0 frequency arise from these different interactions.

3.1.3 Function

The taxonomic substates exemplify how proteins can tune their functional properties in response to external influences. They rebind CO with different rates, A_0 being the fastest and A_3 the slowest (Fig. 2a). Dynamic biological control may be exerted by changing relative populations of the A substates. The overall association rate at physiological temperatures, where the A substates are in fast interconversion, can be written as

$$\lambda = \sum_{i=0,1,3} c_i \lambda_i, \tag{5}$$

where the c_i are the fractional populations and the λ_i the overall association rate coefficients of the substates A_i. Equation 5 is an approximation that neglects the (weak) influence of the protonation of His97 on λ.

To include the protonation of His97, we use a model of two non-interacting protonation sites [22]. Fig. 8 a shows experimental data of the pH dependence of λ together with a fit to the expression,

$$\lambda(\mathrm{pH}) = \lambda_{00} + \Pi(\mathrm{pK}_{64})\Delta\lambda_{64} + \Pi(\mathrm{pK}_{97})\Delta\lambda_{97}, \tag{6}$$

with

$$\Pi(\mathrm{pK}) = \frac{1}{1 + 10^{\mathrm{pK}-\mathrm{pH}}}. \tag{7}$$

Here λ_{00} is the high pH rate coefficient, which is practically the population-weighted average rate coefficient of A_1 and A_3. Π is the Henderson-Hasselbalch function that

gives the fraction of sites that are protonated, $\Delta\lambda_{64}$ and $\Delta\lambda_{97}$ are the changes in the on-rate due to the respective residues, with best-fit pK values of 4.2 and 6.1.

3.2 Statistical substates

So far, we have focused on the highest tier of the hierarchy, CS0, that comprises only a few substates. These substates can be characterized individually, and they are amenable to detailed structure-dynamics-function analysis. We now turn to the lower tier substates, sketched crudely in Fig. 1. Actually, the existence of substates was first found in one of the lower tiers: Rebinding of CO and O_2 to myoglobin at temperatures below about 200 K is nonexponential in time. This observation was explained by assuming that Mb could exist in a very large number of slightly different structures with different activation enthalpies [36]. The name *conformational substates* was introduced a few years later [37]. An example of the smooth, nonexponential time dependence is shown in Fig. 2. The number of CS required to describe these kinetics is so large that they can no longer be characterized individually. Their properties must be described by distributions, and we therefore call them *statistical substates.* Initially, we assumed that protein dynamics could be explained with only one tier of CS. This simple notion was shattered by a closer look at many data, and it became clear that substates are arranged in a hierarchy [6,7]. In biomolecular physics, as in all other branches of physics, the detailed exploration of the energy landscape is a necessary step towards a deep understanding of the system under study. Despite years of experimental, theoretical, and computational work by many groups since the suggestion of a hierarchy, we still have only a rudimentary picture. There is no agreement how the tiers should be arranged and classified. Below we discuss some of the relevant questions.

3.2.1 How to characterize tiers?

The first question concerns the characterization of substates. Which properties can we hope to determine so that we get a picture of the energy landscape? In atomic, nuclear, and particle physics, the answer is clear and well known. Energy levels are labeled by their excitation energies (or masses) and the relevant quantum numbers; establishing the connection with other properties is in principle straightforward because they are usually *taxonomic* and can be studied individually. The situation is much more complex in rugged landscapes. A one-dimensional cross section through such a landscape in a single tier is sketched in Fig. 9 a. E_i denotes the height of a barrier between two CSi, and cc$i$ is a conformational coordinate. In principle, the full landscape can

be studied by computer calculations. In practice, however, complete characterization of the energy landscape is a challenging task even for short peptide chains [38,39]. Molecular dynamics (MD) simulations and normal mode analysis provide important insights [40–42], but they have serious limitations. MD simulations extend only up to a few nanoseconds, and the barrier heights explored are consequently restricted. Moreover, the potentials used in the calculations may not be adequate. Simulations on simplified models extend to longer times, but give less detailed information [43,44]. Experimental studies are consequently essential.

Fig. 9 a suggests what can be measured and what kind of measurements are needed. The simplest characterization of the landscape consists of the average barrier height, $\langle E \rangle$, the distribution of barrier heights, $g(E_i)$, and the shape or curvature of the envelope. The barrier height and the distribution can be studied either by observing fluctuations (F) or relaxation phenomena (R), as indicated in Fig. 9 a. In both cases, fluctuations and relaxations, a transition rate coefficient, $\kappa(T)$, is measured as a function of temperature. Here a problem arises: Should we use Eq. 3 or Eq. 4 to analyze the temperature dependence of $\kappa(T)$? Both relations yield a preexponential factor and an activation energy. (Actually, instead of Eq. 4, the Kramers equation should be used [45,46]). Oversimplified, it can be said that Eq. 3 describes a reaction in a rough potential, where E_F is a measure of the roughness of the potential, whereas Eq. 4 describes a transition over a smooth potential barrier. The two relations should actually be combined [30,47]. Consequently, the temperature dependence of $\kappa(T)$ indicates if the energy surface in a given tier is smooth or rough. If Eq. 4 fits the experimental data over a broad temperature range, we assume that the surface roughness is small compared with the barrier height. If the data deviate markedly from Eq. 4, we conclude that the surface is rough. A second hint comes from the preexponential factor A: If A in an Arrhenius analysis is markedly larger than 10^{13} s^{-1}, Eq. 4 is inadequate. Here we will remain old-fashioned and use the Arrhenius equation, Eq. 4, for the characterization of the tiers.

3.2.2 Barrier distributions and hierarchy

Relaxation and fluctuation phenomena in proteins span a range of more than 15 orders of magnitude in time, from less than picoseconds to more than kiloseconds. This wide range of characteristic times arises from a distribution of different energy barriers, $g(E)$, which specifies the probability of finding a barrier with height between E and $E + dE$. Two extreme cases of $g(E)$ are plotted in Fig. 9 b and 9 c as a function of log E. In one extreme case, Fig. 9 b, there is just one broad distribution extending over at least three orders of magnitude in E. Such a broad, continuous distribution

may occur in spin glasses. In the case of a unimodal distribution, the arrangement of substates in the energy landscape may or may not be hierarchical. In the other extreme, Fig. 9 c, a set of narrower distributions occurs at various ranges of barrier heights, corresponding to different tiers in the energy landscape. The individual distributions can be characterized by their average barrier heights, their widths, and the corresponding preexponential factors in Eq. 4. It is clear that myoglobin is characterized by a hierarchical energy landscape, but the number of tiers, their organization and properties, and their connection to the protein structure remain to be explored in detail.

3.2.3 Experimental tools

No single experimental tool alone can explore the energy landscape of a protein completely. A wide variety of techniques is needed to get more than a glimpse. At present, many different approaches have already yielded tantalizing hints of the unexpected complexity of the EL in proteins and the dynamics, but a synthesis of the various results is lacking. We do not attempt such a synthesis here but sketch some of the techniques that have already given useful results and that promise to contribute to an integrated picture.

Time-resolved spectroscopy. The nonexponential rebinding of CO to Mb after flash photolysis at temperatures below 200 K was the first unambiguous evidence for the existence of CS [36]. The nonexponential behavior is seen not only in the CO binding to wild-type swMb, but also in the binding of various ligands to mutated swMb [20,48], and to many other proteins such as horse Mb [49,50], elephant Mb [51], isolated hemoglobin chains [52], leghemoglobin [53], horseradish peroxidase [54], azurin [55], halocyanin [56], and hemerythrin [57]. Laser-induced electron transfer reactions in bacterial reaction center proteins (RCs) also give evidence for the existence of CS and provide a superb method to study the EL in membrane proteins [71]. In summary, these experiments all demonstrate that the existence of CS is a general phenomenon. It is clear that the number of these substates is very large and hence must be described statistically.

Differential scanning calorimetry (DSC) [58]. In DSC, the protein sample is cooled to a temperature near 100 K. Upon heating, the specific heat is measured as a function of temperature at a fixed heating rate. The experiments show a gradual build-up of excess heat starting at about 150 K and continuing up to the denaturation temperature [59–62]. The observation is explained by activation of substate transitions and provides evidence for an exceptionally broad distribution of relaxation times and for widely different heights of barriers between CS. The results give strong support to a

hierarchical arrangement of substates within substates.

Spectral hole burning [63,64]. Proteins in different CS usually have also different energies, and their spectral lines possess somewhat different frequencies [8,65,66]. Spectral lines in proteins are consequently often inhomogeneously broadened; they are Voigtians - Gaussian superpositions of Lorentzians. Information on the EL is obtained by shining a narrow laser line onto a broad protein band. The light burns "holes" in the spectrum by photon-induced transitions of proteins to other CS. These experiments give clear evidence of CS [67]. By studying hole recovery after temperature cycling [68,69] or by observing stimulated photon echoes [70], information on barrier heights has been obtained.

Relaxation techniques. Relaxation methods offer possibly the most general approaches to the study of energy landscapes. By applying an external perturbation, the protein is brought into a non-equilibrium state, as indicated in Fig. 9 a. After removal of the perturbation, the relaxation towards equilibrium can be studied, which yields information about the barriers surmounted. The non-equilibrium state can be reached, for instance, by a laser flash that breaks a bond [6] or initiates transfer of an electron [71], by irradiating the sample with x-rays to produce free electrons [72], or by a pressure [14], temperature, or pH jump. The relaxation process can extend over many orders of magnitude in time [73]. To determine the topography of the energy landscape, measurements as a function of temperature are crucial – but they are often omitted.

Other techniques. There are many other techniques that have played an important role in the exploration of the energy landscape of proteins in the past and are likely to continue to do so in the future, such as x-ray crystallography, Mössbauer spectroscopy, incoherent neutron scattering, magnetic resonance (EPR/NMR), hydrogen exchange, fluorescence spectroscopy and vibrational spectroscopy (infrared absorption and Raman scattering). For a brief description of the application of these techniques to protein dynamics, we refer the reader to a recent review [11].

3.2.4 A glimpse at myoglobin

There is no protein for which the energy landscape has been fully explored. Myoglobin is probably the best studied case. We will sketch some of the present knowledge here but stress that we are still far from a complete understanding. In the first introduction of the hierarchy of substates [6], four different tiers were described, based on the results of a number of different experiments. Later it turned out that the interpretation of one of the experiments, the apparent shift of band III, a charge transfer transition near 760 nm, was incorrect. The shift was not caused by a relaxation process, but

by kinetic hole burning. The basic idea of a hierarchy, however, remains correct. Some insight into the present state of our knowledge of the energy landscape in Mb is obtained by plotting the rate coefficients for a number of different relaxation processes as a function of temperature. Such a plot for proteins raises two questions because fluctuation and relaxation processes can be observed from below 1 K to above 300 K. The first question concerns the form of the preexponential factor in the rate law, Eqs. 3 or 4. If data are extrapolated over only small ranges in T, say from 280 to 300 K, it does not matter if we assume the preexponential to be temperature independent or not. Extrapolation from 1 to 300 K, however, depends strongly on this assumption. We have shown earlier that the form $A(T/T_0)$, used in Eq. 4, fits data better [74], and we consequently base extrapolation on Eq. 4. The second question concerns the choice of the form of the temperature axis. If we use $(1/T)$ or $(1/T)^2$, the biologically interesting range from 200 to 300 K is squeezed so that crucial features cannot be recognized. We consequently use two plots. In Fig. 10 a, we show log $\kappa(T)$ versus log T over the entire range from 1 to 300 K. In Fig. 10 b, we plot log $\kappa(T)$ versus $(1/T)$ in the range from 200 to 300 K. The two figures together provide insight into the broad range of relaxation and fluctuation phenomena in Mb. In both figures, measured rate coefficients are indicated by solid lines, those extrapolated with Eq. 4 by dashed lines.

The richness and complexity of the energy landscape emerges when we plot the data for a few relaxation phenomena in Fig. 10. We begin at the lowest temperatures, 2 - 8 K, where the experiments of Thorn Leeson and Wiersma [70] have revealed three processes, denoted by a, b, and c. Their measured rate coefficients are indicated by solid lines in Fig. 10 a. The extrapolation with Eq. 4 is shown as dotted lines in Figs. 10 a and 10 b. Evidence for relaxation processes between 8 and 70 K exists [68], but the relevant rate parameters are not yet known. Above about 100 K, additional relaxation processes are activated [60,72] but more experiments with different tools and over broad ranges of temperature and solvent properties will be needed before definite assignments can be made. A few processes, however, are already well enough studied so that they can be plotted in Fig. 10 and that their structural origin and their functional importance can be discussed. The first of these processes, labeled d in Fig. 10, is the relaxation of metmyoglobin after irradiation by x-rays at 77 K and then increasing the temperature [75]. The relaxation starts at about 140 K and is completed by about 200 K. The exchanges between the taxonomic substates [17,27,76], treated in Section 3.1 and plotted in Fig. 7, also begin below 200 K. The data are again shown in Fig. 10; e is the exchange $A_0 \leftrightarrow A_1 + A_3$ and f denotes the exchange $A_1 \leftrightarrow A_3$. The next process is the Agmon-Hopfield relaxation of the protein after photodissociation, $B^* \rightarrow B$, which increases the barrier for rebinding [8,77]. The relaxation has been measured in various solvents [8,78]. The relaxation in a 75 % glycerol-water solvent is nonexponential in time and can be represented by a stretched exponential, Eq. 2.

The corresponding rate coefficient is plotted as curve g in Fig. 10. Another process that has been examined is the exit of CO [8] from Mb; the rate coefficient is shown as curve h. Additional relaxation phenomena have been observed in many experiments, but few data extend over a broad enough time and temperature range to provide all the information needed to fill in the gaps in Fig. 10.

4 Discussion

Fig. 10 provides only a partical glance at the relaxation phenomena in one simple protein, myoglobin. Many problems remain to be solved before we have a detailed picture of the energy landscape in myoglobin or another "simple" protein. We sketch a few of these problems here. (i) Survey of the existing data on Mb. Here we have only used a small number of the published experiments. A complete survey will indicate where gaps are already filled and where more experiments are needed. (ii) Some of the fluctuations or relaxation processes depend crucially on the viscosity of the solvent surrounding the protein [36,75,77–81]. We have called this effect a "slaved glass transition". The energy landscape of the protein depends on the surrounding; protein and environment must be treated together. (iii) Once more details of the energy landscape are known, its organization can be investigated more closely. Are the various motions independent, are they related, do some motions in lower tiers control motions in higher tiers? How can the motions be arranged logically in a hierarchy? (iv) The relation of motions (or tiers) with structural features must be explored. In one case, the transition $A_0 \rightarrow A_1$, a clear connection has been established: In A_1, the distal histidine is inside the heme pocket, in A_0, it extends into the solvent. The motion hence involves the swinging in and out of the side chain of the distal histidine [25]. (v) The functional significance of the various motions and hence the various tiers of substates remains to be established. The more details emerge from the various experiments, the more it becomes clear that even a simple protein such as Mb is very complex and exhibits a broad range of motions. The data shown here imply that it will take a considerable time before the energy landscape of even one protein is fully explored. The importance of the landscape for an understanding of proteins as physical systems and for understanding them as biological machines is, however, already evident.

Acknowledgments

This work was supported by grant GM 18051 from the National Institutes of Health.

References

[1] L. Stryer, Biochemistry, 4th ed. (Freeman, San Francisco, 1995).

[2] P.L. Privalov, Annu. Rev. Biophys. Biophys. Chem. 18 (1989) 47.

[3] D.L. Stein, Proc. Natl. Acad. Sci. USA 82 (1985) 3670.

[4] G. Toulouse, Commun. Phys. 2 (1977) 115.

[5] R. Palmer, in: Takayama H (ed) Cooperative Dynamics in Complex Physical Systems (Springer, New York, 1988) pp. 118.

[6] A. Ansari, J. Berendzen, S.F. Bowne, H. Frauenfelder, I.E.T. Iben, T.B. Sauke, E. Shyamsunder and R.D. Young, Proc. Natl. Acad. Sci. USA 82 (1985) 5000.

[7] A. Ansari, J. Berendzen, D. Braunstein, B.R. Cowen, H. Frauenfelder, M.K. Hong, I.E.T. Iben, J.B. Johnson, P. Ormos, T.B. Sauke, R. Scholl, A. Schulte, P.J. Steinbach, J. Vittitow and R.D. Young, Biophys. Chem. 26 (1987) 337.

[8] P.J. Steinbach, A. Ansari, J. Berendzen, D. Braunstein, K. Chu, B.R. Cowen, D. Ehrenstein, H. Frauenfelder, J.B. Johnson, D.C. Lamb, S. Luck, J.R. Mourant, G.U. Nienhaus, P. Ormos, R. Philipp, A. Xie and R.D. Young, Biochemistry 30 (1991) 3988.

[9] H. Frauenfelder, S.G. Sligar and P.G. Wolynes, Science 254 (1991) 1598.

[10] G.U. Nienhaus, J.R. Mourant and H. Frauenfelder, Proc. Natl. Acad. Sci. USA 89 (1992) 2902.

[11] G.U. Nienhaus and R. D. Young, in: G. Trigg (ed) Encyclopedia of Applied Physics, Vol. 15 (VCH Publishers, Weinheim, 1996).

[12] W.S Caughey, H. Shimada, M.G. Choc and M.P. Tucker, Proc. Natl. Acad. Sci. USA 78 (1981) 2903.

[13] M.K. Hong, D. Braunstein, B.R. Cowen, H. Frauenfelder, I.E.T. Iben, J.R. Mourant, P. Ormos, R. Scholl, A. Schulte, P.J. Steinbach, A. Xie and R.D. Young, Biophys. J. 58 (1990) 429.

[14] H. Frauenfelder, N.A. Alberding, A. Ansari, D. Braunstein, B.R. Cowen, M.K. Hong, I.E.T. Iben, J.B. Johnson, S. Luck, M.C. Marden, J.R. Mourant, P. Ormos, L. Reinisch, R. Scholl, A. Schulte, E. Shyamsunder, L.B. Sorenson, P.J. Steinbach, A. Xie, R.D. Young and K.T. Yue, J. Phys. Chem. 94 (1990) 1024.

[15] H. Shimada and W.S. Caughey, J. Biol. Chem. 257 (1982) 11893.

[16] M.W. Makinen, R.A. Houtchens and W.S. Caughey, Proc. Natl. Acad. Sci. USA 76 (1979) 6042.

[17] J.B. Johnson, D.C. Lamb, H. Frauenfelder, J.D. Müller, B. McMahon, G. U. Nienhaus and R. D. Young, Biophys. J. 71 (1996) 1563.

[18] J. T. Sage, P. Li and P. M. Champion, Biochemistry 30 (1991) 1227.

[19] S. Han, D. L. Rousseau, G. Giacometti and M. Brunori, Proc. Natl. Acad. Sci. 87 (1990) 205.

[20] D.P. Braunstein, K. Chu, K.D. Egeberg, H. Frauenfelder, J.R. Mourant, G.U. Nienhaus, P. Ormos, S.G. Sligar, B.A. Springer and R.D. Young, Biophys. J. 65 (1993) 2447-2454.

[21] T. Li, M.L. Quillin, G.N. Phillips, Jr., and J.S. Olson, Biochemistry 33 (1994) 1433.

[22] J.D. Müller, E.Y.T. Chien, B. McMahon, S.G. Sligar and G.U. Nienhaus, Biophys. J. 70 (1996) A218.

[23] D. Morikis, P.M. Champion, B.A. Springer and S.G. Sligar, Biochemistry 28 (1989) 4791.

[24] M.L. Quillin, R.E. Brantley, Jr., K.A. Johnson and G. Phillips, Biophys. J. 61 (1992) A466.

[25] F. Yang and G.N. Phillips, Jr., J. Mol. Biol. 256 (1996) 762.

[26] H. Scher, M.F. Shlesinger and J.T. Bendler, Physics Today 44 (1991) 26 (January).

[27] R.D. Young, H. Frauenfelder, J.B. Johnson, D.C. Lamb, G.U. Nienhaus, R. Philipp and R. Scholl, Chem. Phys. 158 (1991) 315.

[28] P.J. Steinbach, K. Chu, H. Frauenfelder, J.B. Johnson, D.C. Lamb, G.U. Nienhaus, T.B. Sauke and R.D. Young, Biophys. J. 61 (1992) 235.

[29] J.D. Ferry, L.D. Grandine, Jr., and E.R. Fitzgerald, J. Appl. Phys. 24 (1953) 911.

[30] J.D. Bryngelson and P.G. Wolynes, J. Phys. Chem. 93 (1989) 6902.

[31] H. Bässler, Phys. Rev. Lett. 58 (1987) 767.

[32] F. Richert and H. Bässler, J. Phys.: Condens. Matter 2 (1990) 2273.

[33] R. Zwanzig, Proc. Natl. Acad. Sci. USA 85 (1988) 2029.

[34] R.D. Young, J. Chem. Phys. 98 (1993) 2488.

[35] P. Ormos, A. Ansari, D. Braunstein, B.R. Cowen, H. Frauenfelder, M.K. Hong, I.E.T. Iben, T.B. Sauke, P.J. Steinbach and R.D. Young, Biophys. J. 57 (1990) 191.

[36] R.H. Austin, K.W. Beeson, L. Eisenstein, H. Frauenfelder and I.C. Gunsalus, Biochemistry 14 (1975) 5355.

[37] H. Frauenfelder, G.A. Petsko, and D. Tsernoglou, Nature 280 (1979) 558.

[38] R. Czerminski and R. Elber, Proc. Natl. Acad. Sci. USA 86 (1989) 6963.

[39] J. E. Straub and D. Thirumalai, Proc. Natl. Acad. Sci. USA 90 (1993) 809.

[40] R. Elber and M. Karplus, Science 235 (1985) 318.

[41] T. Noguti and N. Go, Proteins Struct. Funct. Genet. 5 (1989) 97.

[42] A. E. Garcia, R. Blumenfeld, G. Hummer and J. A. Krumhansl, this issue.

[43] G. Iori, E. Marinari and G. Parisi, Europhys. Lett. 25 (1994) 491.

[44] H. Grubmüller and P. Tavan, J. Chem. Phys. 101 (1994) 5047.

[45] H. Frauenfelder and P.G. Wolynes, Science 229 (1985) 337.

[46] P. Hänggi, P. Talkner and M. Borkovec, Rev. Mod. Phys. 62 (1990) 251.

[47] V.P. Denisov, J. Peters, H.D. Horlein and B. Halle, Nature Struct. Biol. 3 (1996) 505.

[48] T. Li, M.L. Quillin, G.N. Phillips, Jr., and J.S. Olson, Biochemistry 33 (1994) 1433.

[49] F. Post, W. Doster, G. Karvounis and M. Settles, Biophys. J. 64 (1993) 1833.

[50] G.U. Nienhaus, K. Chu, B. McMahon and J.D. Müller, in: Sarma RH and Sarma MH (eds) Biological Structure and Dynamics, Vol. 1 (Adenine Press, Albany NY 1995), pp. 281.

[51] A. Cupane, M. Leone, E. Vitrano, L. Cordone, U.R. Hiltpold, K.H. Winterhalter, W. Yu and E.E. Di Iorio, Biophys. J. 65 (1993) 2461.

[52] N. Alberding, S.S. Chan, L. Eisenstein, H. Frauenfelder, D. Good, I.C. Gunsalus, T.M. Nordlund, M.F. Perutz, A.H. Reynolds and L.B. Sorensen, Biochemistry 17 (1978) 43.

[53] F. Stetzkowski, R. Banerjee, M.C. Marden, D.K. Beece, S.F. Bowne, W. Doster, L. Eisenstein, H. Frauenfelder, L. Reinisch, E. Shyamsunder and C. Jung, J. Biol. Chem. 260 (1985) 8803.

[54] W. Doster, S.F. Bowne, H. Frauenfelder, L. Reinisch and E. Shyamsunder J. Mol. Biol. 194 (1987) 299.

[55] D. Ehrenstein, and G.U. Nienhaus, Proc. Natl. Acad. Sci. USA 89 (1992) 9681.

[56] D. Ehrenstein, M. Filiaci, B. Scharf, M. Engelhard, P.J. Steinbach and G.U. Nienhaus, Biochemistry 34 (1995) 12170.

[57] D. Lavalette and C. Tetreau, Eur. J. Biochem. 177 (1988) 97.

[58] K.J. Breslauer, E. Freire and M. Straume, in: Meth. Enzymol., Vol. 211 (Academic Press, New York, 1992) pp. 533.

[59] W. Doster, A. Bachleitner, R. Dunau, M. Hiebl and E. Lüscher, Biophys. J. 50 (1986) 213.

[60] G. Sartor, E. Mayer and G.P. Johari, Biophys. J. 66 (1994) 249.

[61] J.L. Green, J. Fan and C.A. Angell, J. Phys. Chem. 98 (1994) 13780.

[62] C. A. Angell, Science 267 (1995) 1924.

[63] J. Friedrich, in: Meth. Enzymol., Vol. 246 (Academic Press, New York, 1995) pp. 226.

[64] R. Jankowiak, J.M. Hayes and G.J. Small, Chem. Rev. 93 (1993) 1471.

[65] A. Cooper, Chem. Phys. Lett. 99 (1983) 305.

[66] B.F. Campbell, M.R. Chance and J.M. Friedman, Science 238 (1987) 373.

[67] J. Gafert, J. Friedrich and F. Parak, J. Chem. Phys. 99 (1993) 2478.

[68] A. Kurita, Y. Shibata and T. Kushida, Phys. Rev. Lett. 74 (1995) 4349.

[69] K. Fritsch, J. Friedrich, F. Parak and J.L. Skinner, Proc. Natl. Acad. Sci. USA, in press.

[70] D. Thorn Leeson and D.A. Wiersma, Nature Struct. Biol. 2 (1995) 848.

[71] B. McMahon, J.D. Müller, B. Marino, P. Debrunner, C. Wraight and G.U. Nienhaus, Biophys. J. 70 (1996) A142.

[72] R. Davydov, M. Sahlin, S. Kuprin, A. Gräslund and A. Ehrenberg, Biochemistry 35 (1996) 5571.

[73] M. Lim, T.A. Jackson and P.A. Anfinrud, Proc. Natl. Acad. Sci. 90 (1993) 5801.

[74] D.D. Dlott, H. Frauenfelder, P. Langer, H. Roder and E.E. Di Iorio, Proc. Natl. Acad. Sci. USA 80 (1983) 6239.

[75] V.E. Prusakov, J. Steyer and F.G. Parak, Biophys. J. 68 (1995) 2524.

[76] E. Mayer, Biophys. J. 67 (1994) 862.

[77] N. Agmon and J.J. Hopfield, J. Chem. Phys. 79 (1983) 2042.

[78] A. Ansari, C.M. Jones, E.R. Henry, J. Hofrichter and W.A. Eaton, Biochemistry 33 (1994) 5128.

[79] D. Beece, L. Eisenstein, H. Frauenfelder, D. Good, M.C. Marden, L. Reinisch, A.H. Reynolds, L.B. Sorensen and K.T. Yue Biochemistry 19 (1980) 5147.

[80] I.E.T. Iben, D. Braunstein, W. Doster, H. Frauenfelder, M.K. Hong, J.B. Johnson, S. Luck, P. Ormos, A. Schulte, P.J. Steinbach, A.H. Xie and R.D. Young, Phys. Rev. Lett. 62 (1989) 1916.

[81] S.J. Hagen, J. Hofrichter and W.A. Eaton, J. Phys. Chem. 100 (1996) 12008.

Figure Captions

Fig. 1. Structure and conformational energy landscape of MbCO. Right column: Simplified scheme of the conformational energy, E_c, in three different tiers of the hierarchical energy landscape, as a function of a conformational coordinate, cci. Note that in reality, E_c is a hypersurface in a high-dimensional conformational space. Left column (top): Ribbon diagram and sketch of MbCO including a possible binding path of the CO ligand from the solvent (S) to the pocket (B) and the iron binding site (A); (middle) infrared spectrum of the stretch bands of heme-bound CO, showing three bands that are assigned to the three taxonomic substates A_0, A_1, and A_3 in the right column of the figure; (bottom) Mean-square displacements of amino acids (backbone averages N, C_α, C) of met-Mb at 300 K (upper) and 80 K (lower) as a function of residue number.

Fig. 2. Flash photolysis rebinding of MbCO ($\approx$20 mM in 75 % glycerol/buffer, pH 5.8). (a) Dots: Kinetics at 120 K monitored separately in the three different infrared stretch bands of CO bound to Mb. $N(t)$ is the fraction of protein molecules that have not rebound the ligand at time t after photodissociation. Dashed line: Exponential. (b) The barrier distributions, $g(H_{BA})$, of the individual A states, connected to the kinetics by $N(t) = \int g(H_{BA}) \exp[-k(A_{BA}, H_{BA}, T)t] dH$, with $k(A_{BA}, H_{BA}, T)$ given by Eq. 4.

Fig. 3. Infrared spectra of CO bound to sperm whale myoglobin in aqueous buffer solution, measured as a function of pH. (a) Measured spectra, normalized to 1 OD cm^{-1}; (b) basis spectra obtained from a fit with the two-site titration model, shown in Fig. 5 a. The measured spectra are a linear combination of the basis spectra with pH-dependent amplitudes given by the fractional populations of Fig. 5 b. The doubly protonated, low-pH form (S_{11}) peaks at 1966 cm^{-1}. The leftmost spectrum corresponds to the unprotonated form (S_{00}), whereas the intermediate one represents a mixture of the two singly protonated species (S_{01} and S_{10}) according to their relative populations.

Fig. 4. Structure of MbCO at the active site (pH 6) [25]. The two protonating histidines, His64 and His97, are plotted with heavier lines. The heme is shown side-on in the center.

Fig. 5. (a) Schematic of the two-site titration model. The indices of the protein sub-

state S_{ij} specify the charge of His64 and His97, respectively. The number 0 indicates the neutral form, while 1 represents the positively charged amino acid. The equilibrium between two adjacent states is described by the Henderson-Hasselbalch equation, Eq. 7. (b) Fractional populations of the four protonation species, as a function of pH, with a pK of 6.0 for His97 and 4.5 for His64.

Fig. 6. Flash photolysis kinetics of MbCO (≈20 mM in 75 % glycerol/buffer, pH 5.8) monitored separately in the A_0 and A_1 substates; squares: 230 K, diamonds 240 K, triangles (tip up) 250K, triangles (tip down) 260 K.

Fig. 7. Logarithmic plot of the characteristic rate coefficients for the transitions $A_1 \leftrightarrow A_3$ and $A_0 \leftrightarrow (A_1 + A_3)$ as a function of $(1000/T)^2$, showing data from flash photolysis and pressure release experiments on MbCO (≈20 mM in 75 % glycerol/buffer, pH 5.8). The straight line is the best fit of the Ferry law, Eq. 3, to the data.

Fig. 8. Association rates of MbCO after flash photolysis at 296 K, CO pressure = 1 atm. (a) Diamonds: experimental data; solid line: fit with a two-site protonation model ($\lambda/s^{-1} = 592 + 4040\Pi(4.2) + 58\Pi(6.1)$, where Π(pK) is given by Eq. 7; (b) to show the third term in the equation in both data and model, the first two terms ($592 + 4040\Pi(4.2)$) have been subtracted from the experimental data and the total calculated curve in panel (a).

Fig. 9. (a) Sketch of a rugged conformational energy landscape. For relaxation (R) and fluctuation (F) processes, energy barriers of height E have to be surmounted. Two limiting barrier distributions, g(E); (b) distribution consisting of a set of discrete distributions, (c) continuous distribution of barriers.

Fig. 10. Rate coefficients for some fluctuation and relaxation phenomena in myoglobin. The processes a to c have been observed in laser hole burning; d is the relaxation of met Mb after x-ray irradiation, e and f are transitions between taxonomic substates; g denotes the Agmon-Hopfield relaxation $B \rightarrow B^*$; h characterizes the exit of CO from the heme pocket. For details, see the text.

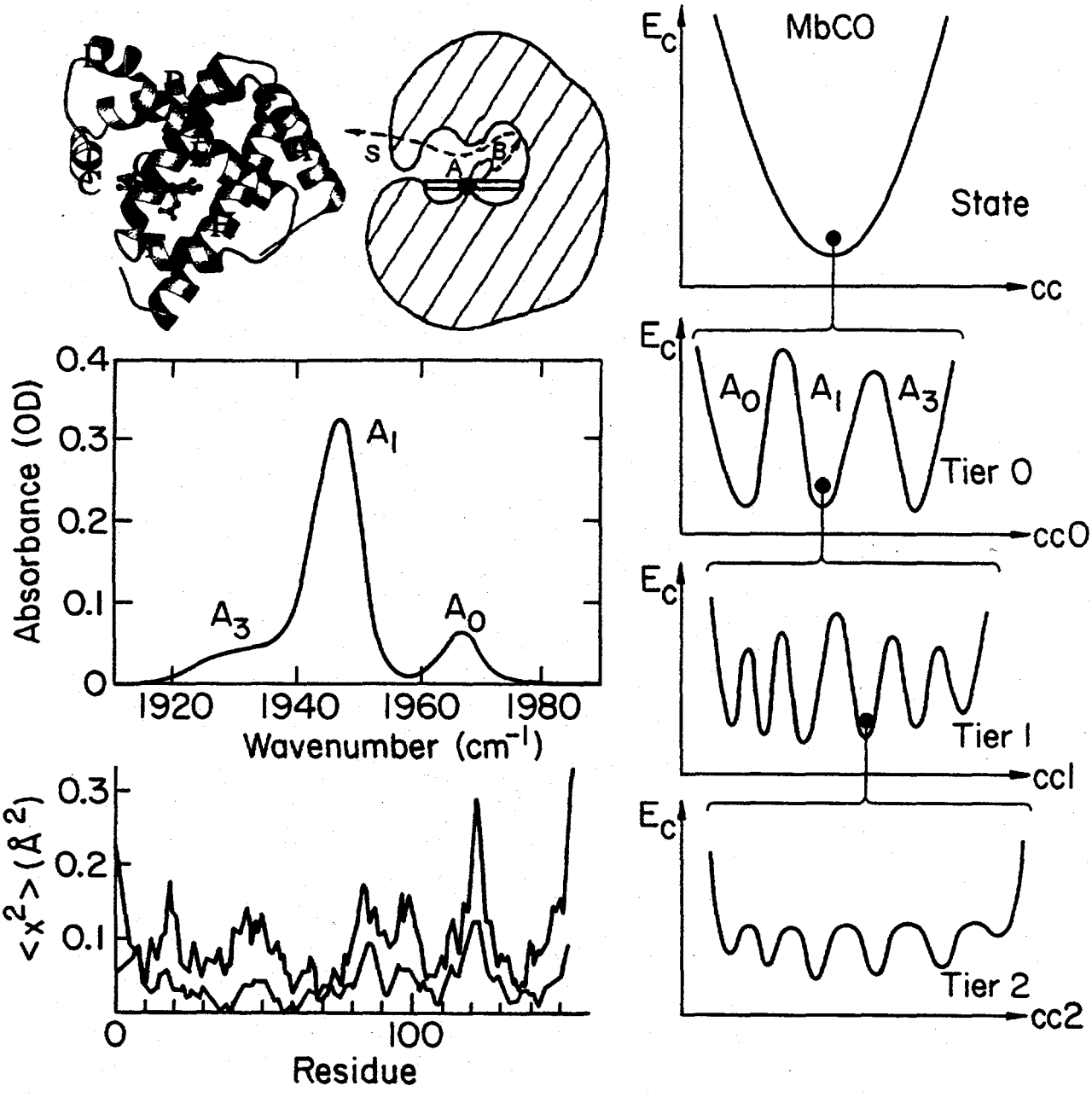
S
A
B
Absorbance (OD)
0.4
0.3
0.2
0.1
0
A1
A3
A0
1920
1940
1960
1980
Wavenumber (cm-1)
<x2> (Å2)
0.3
0.2
0.1
0
100
Residue
Ec
MbCO
State
cc
A0
A1
A3
Tier 0
cc0
Tier 1
cc1
Tier 2
cc2

Fig. 1

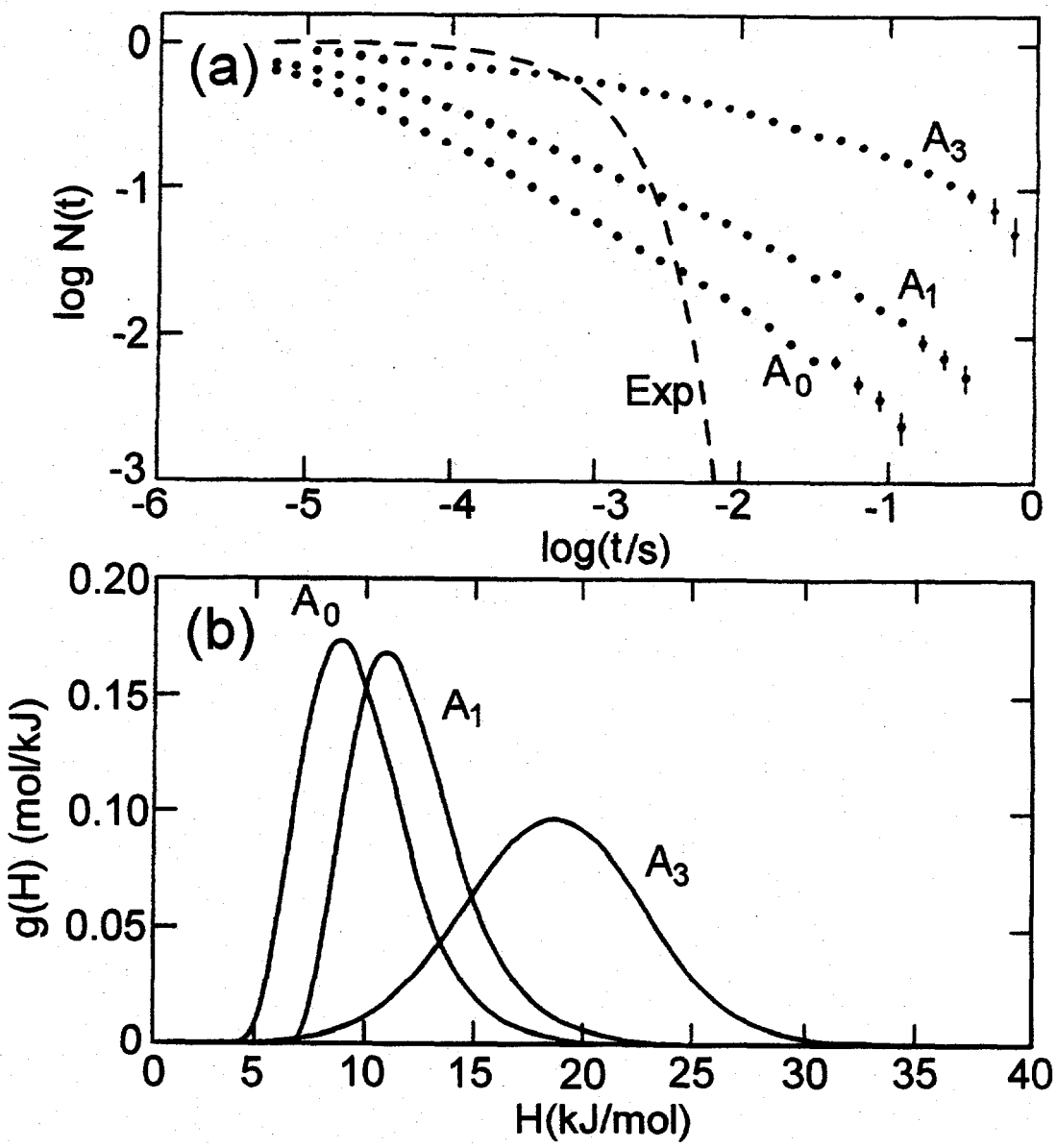
(a)
log N(t)
0
-1
-2
-3
-6
-5
-4
-3
-2
-1
0
log(t/s)
A3
A1
A0
Exp
(b)
g(H) (mol/kJ)
0.20
0.15
0.10
0.05
0
0
5
10
15
20
25
30
35
40
H(kJ/mol)
A0
A1
A3

Fig.2

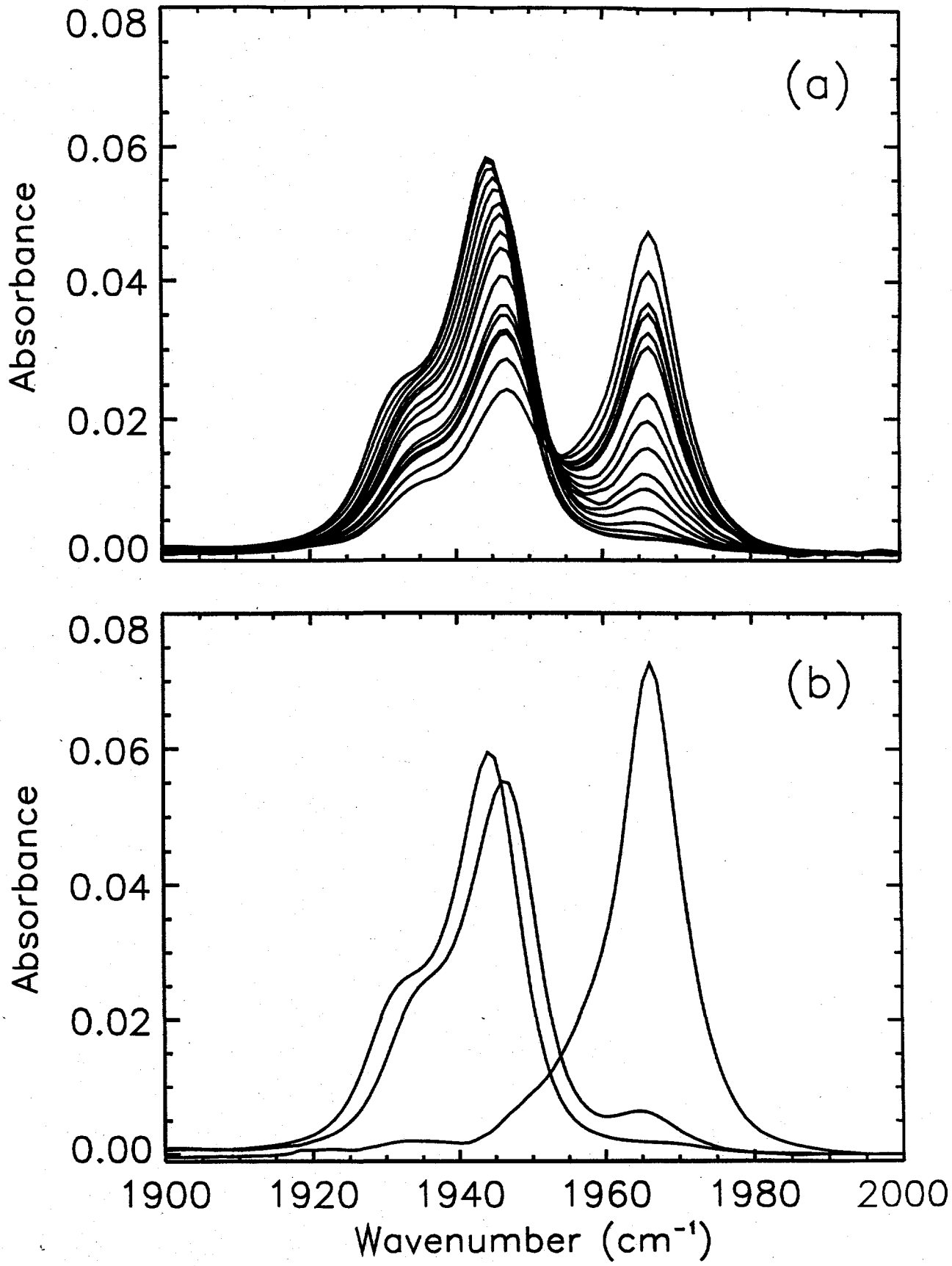
(a)
(b)
Absorbance
0.08
0.06
0.04
0.02
0.00
1900
1920
1940
1960
1980
2000
Wavenumber (cm⁻¹)

Fig.3

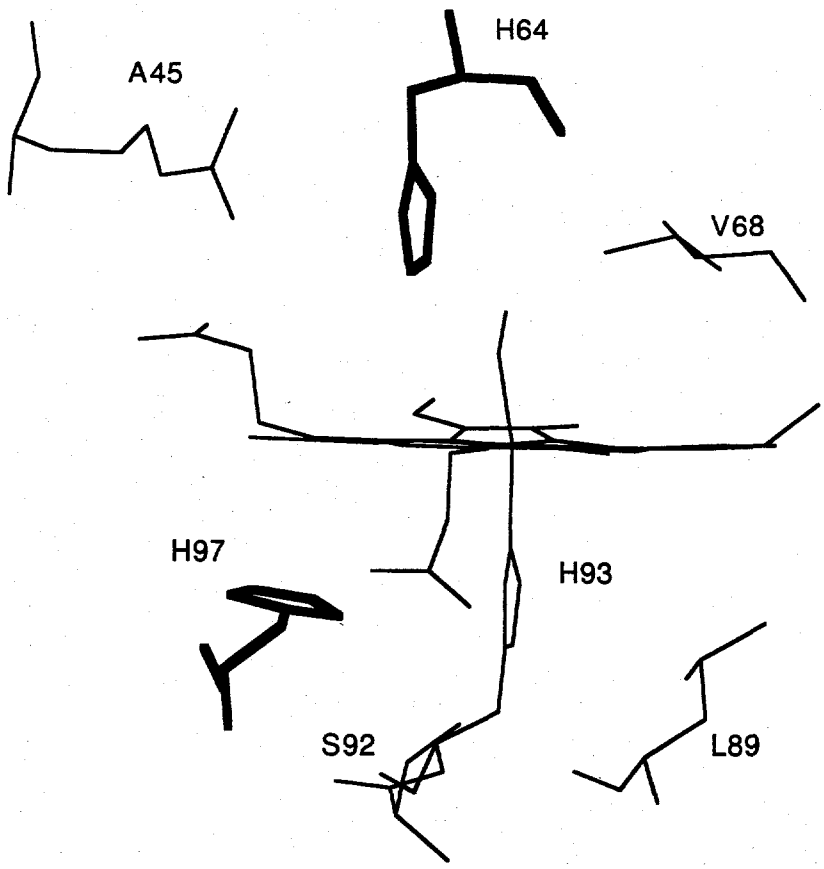

Fig. 4

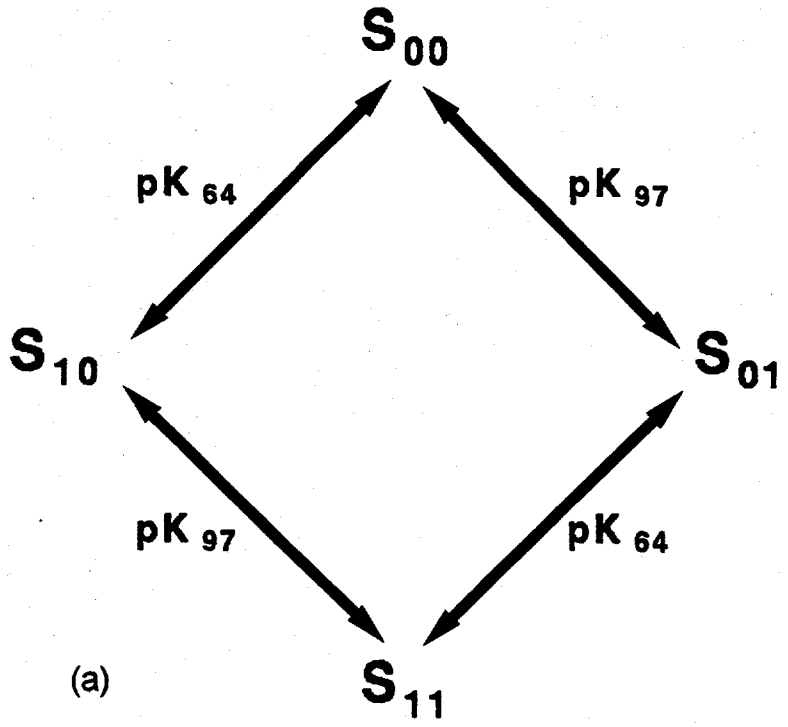
S00
pK 64
pK 97
S10
S01
pK 97
pK 64
S11
(a)

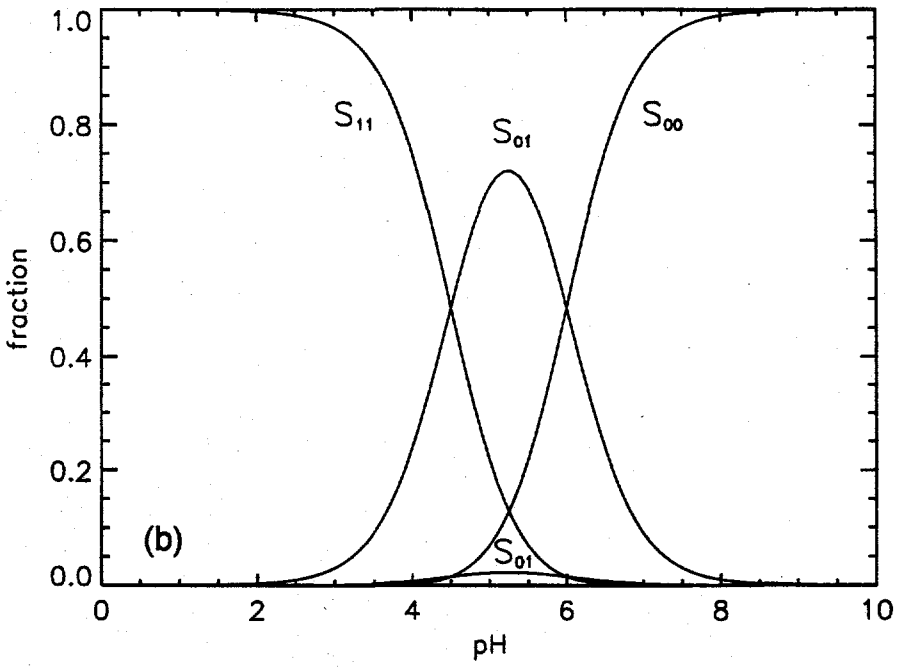
1.0
0.8
0.6
0.4
0.2
0.0
fraction
S11
S01
S00
(b)
S01
0
2
4
6
8
10
pH

Fig. 5

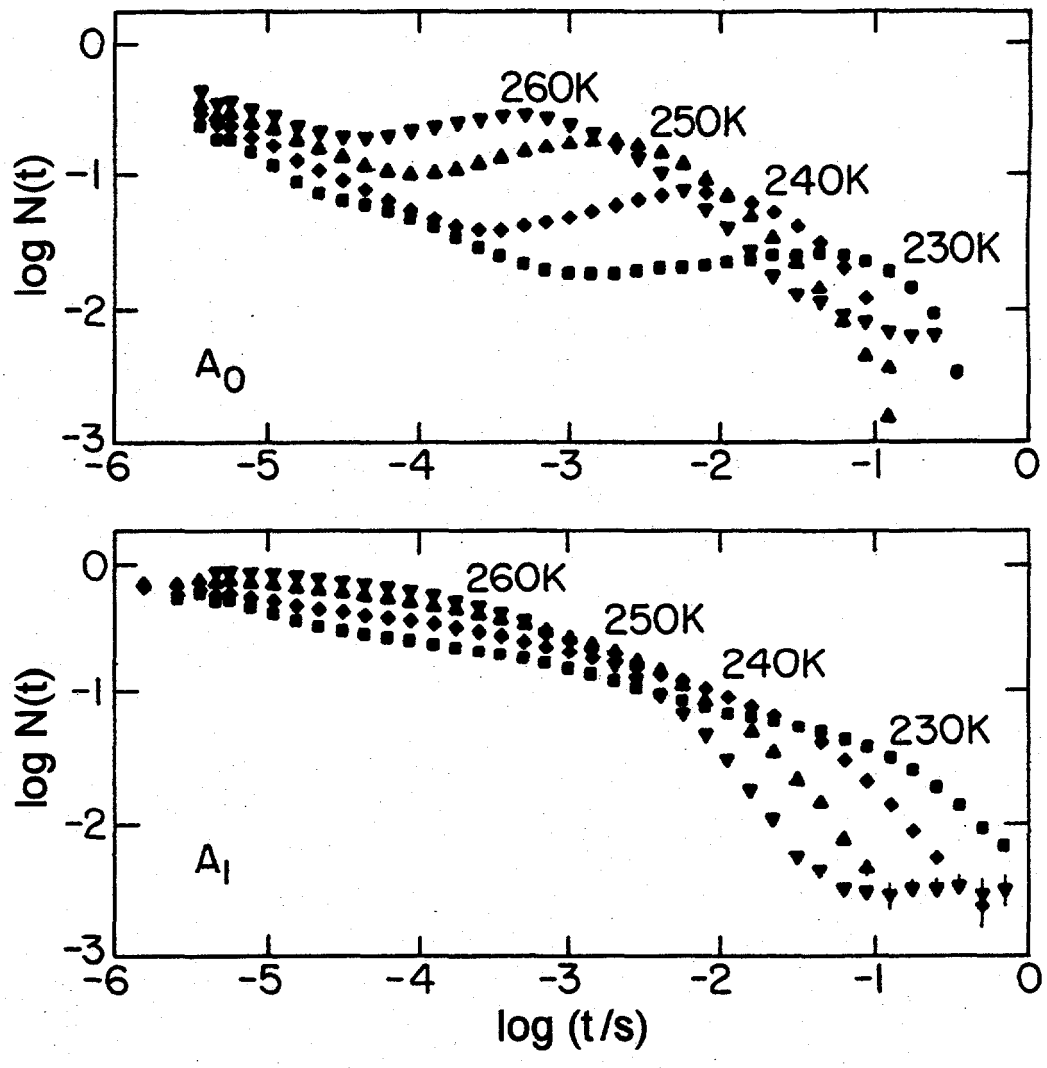
0
-1
-2
-3
log N(t)
260K
250K
240K
230K
A_0
-6
-5
-4
-3
-2
-1
0
0
-1
-2
-3
log N(t)
260K
250K
240K
230K
A_1
-6
-5
-4
-3
-2
-1
0
log (t/s)

Fig. 6

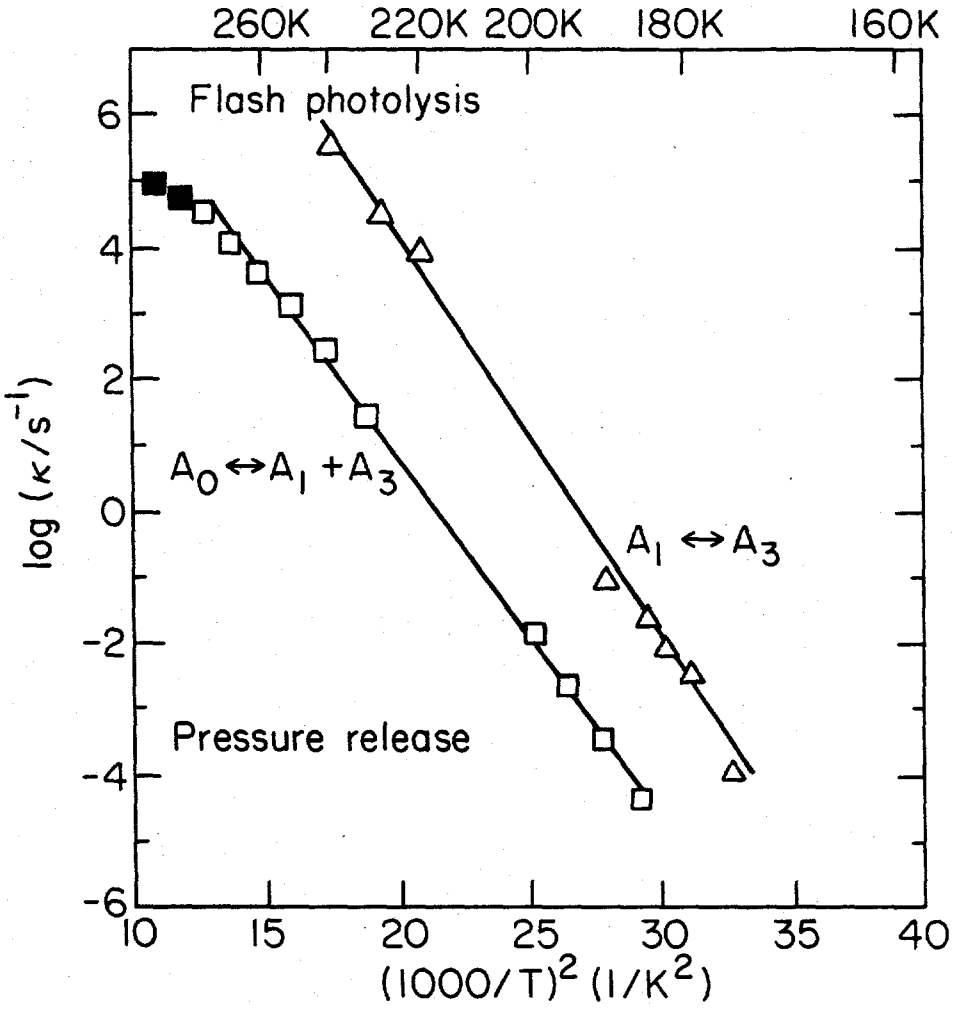
260K
220K
200K
180K
160K
Flash photolysis
$A_0 \leftrightarrow A_1 + A_3$
$A_1 \leftrightarrow A_3$
Pressure release
log (κ/s^{-1})
6
4
2
0
-2
-4
-6
10
15
20
25
30
35
40
(1000/T)^2 (1/K^2)

Fig. 7

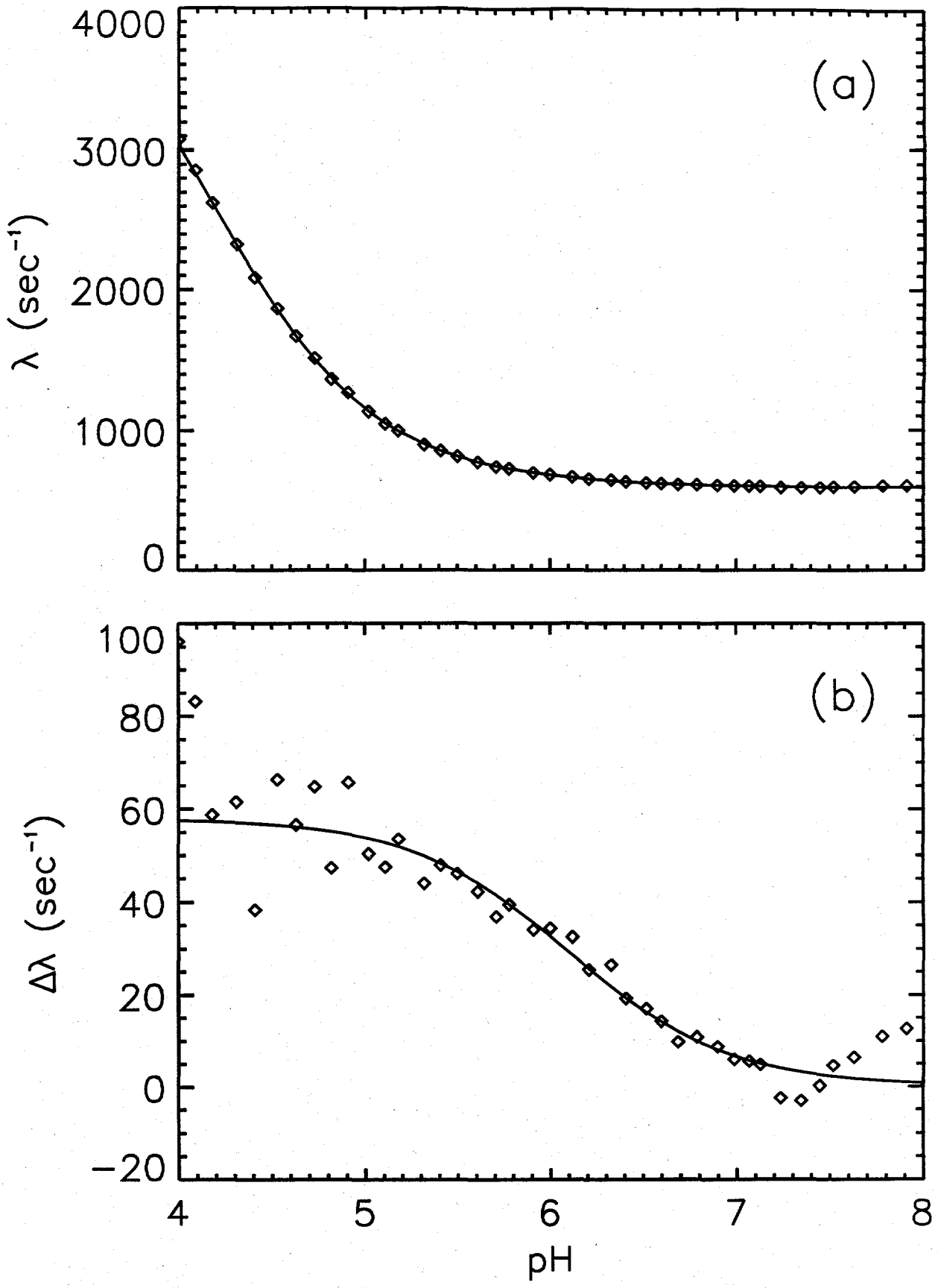
(a)
4000
3000
2000
1000
0
λ (sec⁻¹)
(b)
100
80
60
40
20
0
−20
Δλ (sec⁻¹)
4
5
6
7
8
pH

Fig. 8

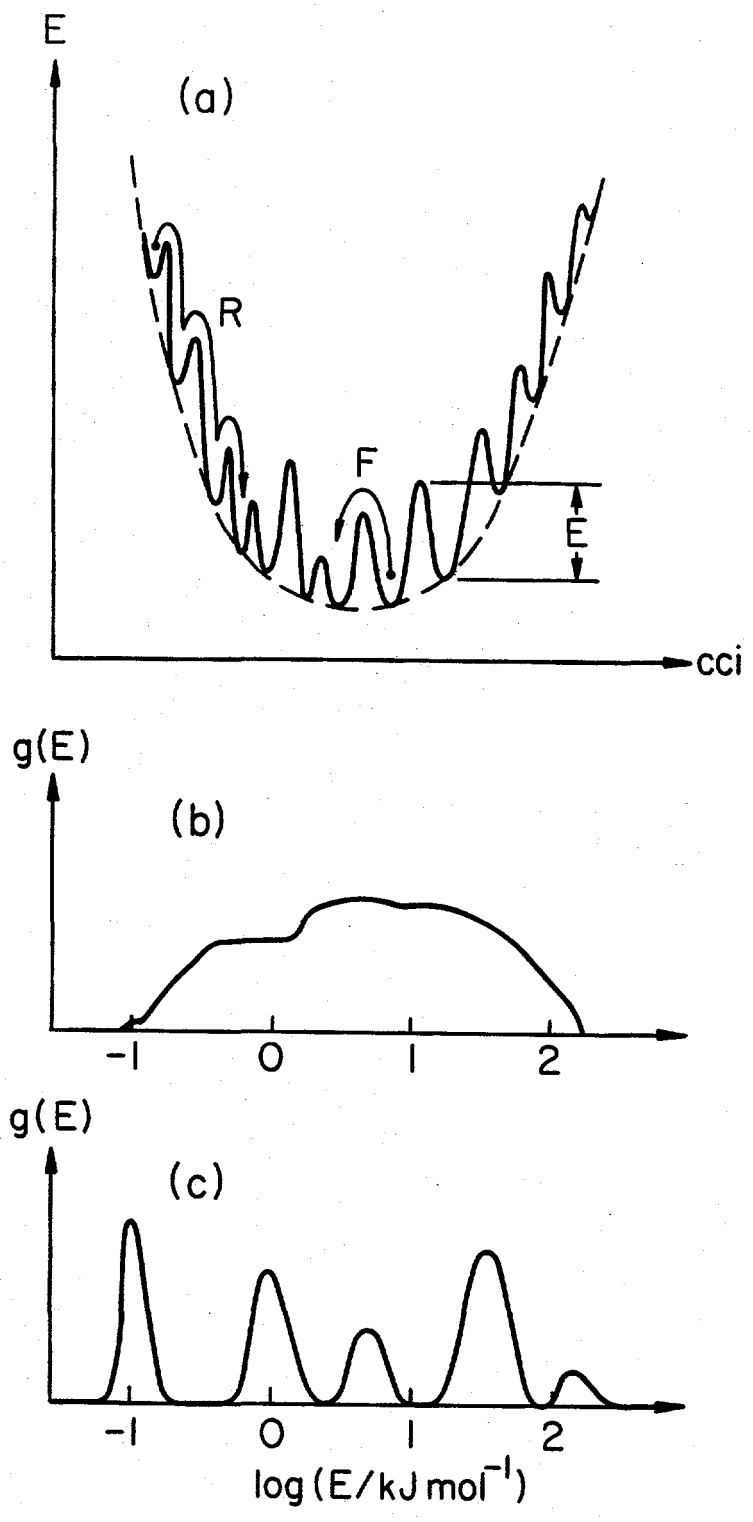

Fig.9

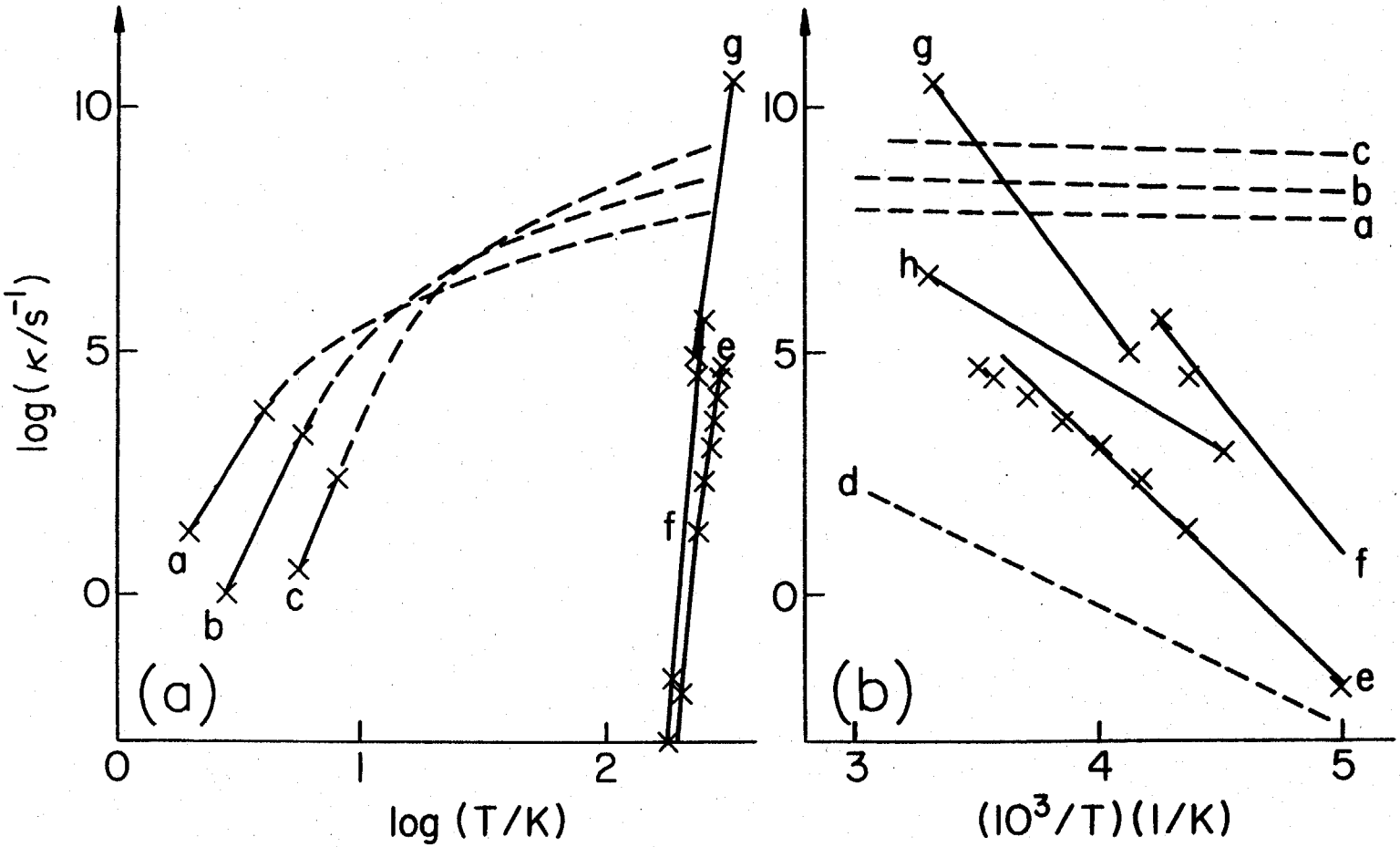

Fig.10